Analysis and modeling of cancer drug responses using cell cycle phase-specific rate effects

Sean M. Gross[1], Farnaz Mohammadi[2], Crystal Sanchez-Aguila[1], Paulina J. Zhan[1], Aaron S. Meyer[2,^], and Laura M. Heiser[1,^,*]

[1]Department of Biomedical Engineering, OHSU Center for Spatial Systems Biomedicine, Knight Cancer Institute, Oregon Health & Science University, Portland, Oregon

[2]Department of Bioengineering, University of California, Los Angeles; Department of Bioinformatics, University of California, Los Angeles; Jonsson Comprehensive Cancer Center, University of California, Los Angeles; Eli and Edythe Broad Center of Regenerative Medicine and Stem Cell Research, University of California, Los Angeles

^Co-corresponding authors

*Lead Contact:

Laura M. Heiser

Department of Biomedical Engineering

2730 S. Moody Ave. CL3G

Portland, OR 97201

Email: heiserl@ohsu.edu

Key words: cell cycle, live-cell imaging, dose response, drug combinations, cancer

ABSTRACT
A major challenge to improving outcomes for patients with cancer is the identification of effective therapeutic strategies that can prevent tumor cell proliferation. Here we sought to gain a deeper understanding of how anti-cancer agents modulate cell cycle progression in HER2+ breast cancer, a disease subtype that accounts for 20% of all breast cancers. We treated HER2+ breast cancer cells with a panel of drugs and tracked changes in cell number and cell cycle phase, which revealed drug-specific cell cycle effects that varied across time. This suggested that a computational model that could account for cell cycle phase durations would provide a framework to explore drug-induced changes in cell cycle changes. Toward that goal, we developed a linear chain trick (LCT) computational model, in which the cell cycle is partitioned into subphases that faithfully captured drug-induced dynamic responses. The model inferred phase-specific drug effects and independent modulation of cell cycle phases, which we confirmed experimentally. We then used our LCT model to predict the effect of unseen drug combinations that target cells in different cell cycle phases. Experimental testing confirmed several model predictions and identified combination treatment strategies that may improve therapeutic response in patients with HER2+ breast cancer. Overall, this integrated experimental and modeling approach opens new avenues for assessing drug responses, predicting effective drug combinations, and identifying optimal drug sequencing strategies.

INTRODUCTION

The mammalian cell cycle can be separated into four linked phases (G_1, S, G_2 and M) with multiple check points (restriction point, DNA damage checkpoint, and the spindle assembly checkpoint)[1–4]. Cell cycle phases and checkpoints are primarily composed of different molecular entities and, consequently, each phase is regulated in different ways, which results in minimal correlation between cell cycle phase durations in individual cells[5]. This independence between phases and checkpoints has implications for cancer treatment because many cancer drugs directly target different aspects of the cell cycle; for example, CDK4/6 inhibitors block progression out of G_1 phase[6], while the nucleoside analog gemcitabine activates the DNA damage checkpoint by targeting DNA synthesis during S-phase[7]. Together, these findings imply that drug-induced changes to cell numbers can be achieved through distinct cell cycle dependent molecular mechanisms.

Developing transformative anti-cancer therapies will require identification of effective drug combinations[8–12]. We hypothesized that incorporating information about how individual drugs impact cell cycle behavior can lead to improved predictions about drug combination effects. For example, it is reasonable to assume that two drugs that reduce the rate of G_1 progression would not increase cell death when combined but instead would lead to deeper reductions in the rate of G_1 progression. At subsaturating doses these effects would likely add together to reduce cell numbers, but at higher saturating doses the cell number would likely peak at the maximum cytostatic effect. This general idea of drug combination efficacy was recently explored in a study of the multi-drug CHOP protocol, which showed that the effectiveness of this drug combination could be attributed to the fact that each agent had non-overlapping cytotoxic effects[13]. Thus, considering both cell cycle and cell death effects in greater detail has the potential to significantly improve drug combination predictions.

xThe classic approach to quantify cancer drug response is to calculate the number of cells 72 hours after drug treatment when cells are assumed to be in exponential growth[14–17]. Recent advances in methodological and quantitative approaches enable assessment of growth rates rather than static cell counts[18,19]. These growth rate approaches significantly improve quantification but provide limited information about cell cycle effects. Fractional proliferation, which models the number of cycling, quiescent, and dying cells in a drug treated population, incorporates growth rates and assumes that cells irreversibly exit the cell cycle into quiescence[20]. These prior studies suggest that a complete understanding of therapeutic response and resistance will require consideration of the diverse mechanisms by which anti-cancer drugs modulate cell numbers.

In this report, we quantify and incorporate cell cycle phase effects in an analysis of responses to single drugs and drug combinations. We used live-cell imaging of AU565 HER2+ breast cancer cells engineered to express a cell cycle reporter and tracked the dynamics of cell number and cell cycle phase in response to single drugs and drug combinations. Across single drugs, we observed distinct routes to similar final cell numbers with phase-specific responses that appear oscillatory over time due to the waiting time effects of the cell cycle. To describe these responses, we developed a computational model that uses a linear chain trick (LCT) to account for the delay effects of cell cycle phase transit upon drug treatment. This LCT model correctly inferred single drug responses across time as well as drug-induced oscillatory cell cycle dynamics. We used this model to predict the effect of unseen combinations of drugs that impact different aspects of the cell cycle. We experimentally tested a number of drug combinations to validate that responses were primarily determined by the specific cell cycle effects of each drug pair. These studies reveal the complexity of cell behavior underlying drug responses, provide

mechanistic insights into how individual drugs modulate cell numbers, and yield a framework for how different drugs can be rationally combined and modeled.

RESULTS

Drug treatments induce distinct changes in cell number and cell cycle phasing

To track drug responses in individual cells, we genetically engineered HER2+ AU565 breast cancer cells to stably express the HDHB cell cycle reporter[21] and a nuclear-localized red fluorescent protein (**Fig. 1A,B**). We then treated cells with escalating doses of five drugs commonly used to treat breast cancer (**Fig. 1C**), imaged cells every 30 minutes for 96H, and quantified cell cycle phase and total cell numbers.

We found that each drug effectively reduced cell numbers in a dose-dependent manner (**Fig. 1D**). As expected, paclitaxel, gemcitabine, and doxorubicin led to cytotoxic effects based on the final cell numbers dropping below the starting cell numbers (**Fig. 1D**)[22,23]. In contrast, at the highest doses of palbociclib and lapatinib, the final cell numbers were approximately equal to the starting cell numbers, suggesting cytostatic effects. For each drug, the pattern of cell counts varied across time, and at high doses responses tended to reach a peak and then decline as the duration of drug exposure increased—an effect most marked for 30nM gemcitabine where the relative cell number declined from 1.1 at 48H to 0.5 at 96H (**Fig. 1D**)[9,19].

Next, we sought to identify whether changes in cell numbers arose through modulation of cell cycle phasing. We observed drug- and dose-dependent changes in the fraction of S-G_2 cells, and these changes exhibited a large time dependence (**Fig. 1E**,**F**). For example, lapatinib and palbociclib initially reduced the fraction of cells in S-G_2 phase in a dose-dependent manner, whereas gemcitabine and doxorubicin initially increased this fraction. Of note, intermediate doses of lapatinib (50 nM) and paclitaxel (3 nM) induced oscillating cell cycle responses, with an initial S-G_2 reduction near 30H, followed by a second S-G_2 reduction at 84H. In sum, our approach revealed drug specific cell cycle changes across time, which confirms that these drugs yield similar final numbers through distinct impacts on the cell cycle.

A dynamical model of the cell cycle captures the dynamics of drug response

A common approach to model drug effects is to assume exponential growth that varies as a function of drug dose. This approach, although informative, cannot explain the cell cycle dynamics that we observed[24] and motivated us to develop a dynamical model to capture the observed behavior. As an initial model we defined a system of ordinary differential equations with transitions between G_1 and S-G_2. The parameters of the ODE model were the cell cycle phase progression and death rates, which were assumed to follow a Hill function with respect to drug concentration. This model failed to fit the experimental data of G_1 and S-G_2 cell numbers (**Sup. Fig 3A-E**), and furthermore dynamical systems theory dictates that this model is unable to oscillate under any reasonable parameterization[25].

To address these limitations and capture the observed oscillatory temporal dynamics, we modified our model's assumptions for cell cycle phase durations. We fit the distribution of single cell cycle phase times to an Erlang distribution and applied the observation that cell cycle phase durations are uncorrelated[5] (**Sup. Fig 1A-E**). Based on the properties of the Erlang distribution, we incorporated a "linear chain trick" into our model, which creates Erlang-distributed time delays in the cell cycle phase durations through a mean-field system of ordinary differential equations (ODEs)[26] (**Fig. 2A**). Additionally, we simplified the model by sharing parameters that were not drug specific, such as the number of cell cycle subphases and the initial fraction of cells in G_1 phase, and then we fit all five drug dose responses simultaneously. Incorporation of this component enabled the model to capture the experimentally observed oscillatory cell cycle behavior and cell cycle phase-specific drug effects (**Fig. 2E-F, I-J & Sup. Fig. 2G-L**). (**Sup. Fig. 1F-G**)

To summarize the overall effect of each drug treatment, we compared the average phase durations and cell death probabilities at the control and the half maximum concentration (EC_{50}) for all five drugs (**Fig. 2E-F, I-J**). The biological effects were captured by the model predictions. Lapatinib and palbociclib treatments resulted in longer average G_1 phase durations compared to untreated cells, by approximately 25H when treated with lapatinib and 10H when treated with palbociclib[27,28] (**Fig. 2E-F**). Moreover, the model inferred a 10% higher chance of cell death in G_1 phase for lapatinib treated cells, and a slight chance of cell death in S-G_2 after palbociclib treatment (**Fig. 2I-J**). The model inferred that cells treated with gemcitabine spent an average of at least 5H more in S-G_2 and have an 8% greater chance of cell death in S-G_2 phase as compared to untreated cells. A 10% chance of cell death at the EC_{50} concentration (2.4 nM) was inferred in late G_2 phase for cells treated with paclitaxel as compared to untreated controls (**Fig. 2J and Fig. S2J**). Overall, our LCT model correctly inferred the known effects of these compounds, suggesting it could be used to design effective anticancer therapy combinations.

Analysis of single cell responses confirms model inferences and reveals drug-specific cell cycle phase effects

The model parameters were developed from the average population response at each timepoint, an experimental approach that enables collection of large numbers of cells. However, the LCT model infers properties of drug response that we can verify by monitoring individual cells. We therefore assessed model inferences at the single-cell level by manually tracking cells to quantify cell cycle phase durations for the first complete cell cycle as well as cell death events (**Fig. 3A**, **Sup. Fig. S3**). The model inferred that the predominant lapatinib effect was to extend G_1 durations from 22.3H in the untreated condition to 33.6H and 47.4H for 25 nM and 50 nM lapatinib, respectively (**Fig. 3A).** Experimentally, we observed that G_1 durations increased after lapatinib (mean 26.2H and 32.5H with 25 and 50 nM lapatinib, respectively) (**Fig. 3A**, **B**). We also quantified an increase in the G_1 duration variance showing that cells varied in their responsiveness to lapatinib (**Fig. 3B**). The model inferred minimal changes to S-G_2 durations or cell death and we accordingly observed little change in S-G_2 durations or cell death in the experimental data (**Fig. 3C**,**D**).

The model inferred that oscillations in the percentage of G_1 cells after lapatinib treatment arise from waiting time effects in cell cycle progression (**Fig. 2**). To confirm the mechanism underlying this behavior at the single cell level, we examined various cell cycle measures and found a reduction in the fraction of cells undergoing their first division beginning around 24H (**Fig. 3E**). This observation, together with the lengthening of the subsequent G_1 duration following cell division (**Fig. 3B**), can explain the cell cycle synchronization observed in Figure 1 and also in the model. At the start of the assay, cells in G_1 are delayed in their time to division, while cells in S-G_2 only become delayed at the onset of G_1 following division. In effect this creates two cohorts of cells with distinct timing in the induction of drug effects.

For gemcitabine, the model inferred a slight acceleration of G_1 phases, which we also observed experimentally (**Fig. 3A**,**F**). The model inferred that S-G_2 durations were extended following gemcitabine treatment, which we confirmed experimentally: S-G_2 durations were extended from 22.3H to 34.5H with 5 nM and to 38H with 10nM gemcitabine (**Fig. 3G**). Lastly, the model inferred an increase in the number of cell death events relative to the starting cell number, from 0 in control to 0.57 with 5 nM gemcitabine. At 10 nM gemcitabine the model predicted 1.0 relative cell deaths such that the number of cell death events across 96H was the same as the initial starting cell number (**Fig. 3A**). The experimentally observed values showed similar trends, though with more modest changes in cell numbers (0.14 and 0.41 relative cell numbers for 5 and 10 nM gemcitabine, respectively) (**Fig. 3H**). Overall, we observed similar trends in each of

the parameters as inferred by the model; modest differences were that the model inferred higher cell death and shorter extensions to S-G_2 than we observed experimentally.

We also tested an assumption of the model that G_1 and S-G_2 phases are independent variables, which captures the idea that these are independently regulated at the molecular level. We analyzed G_1 versus S-G_2 durations for individual cells in the control condition, 10 nM gemcitabine, and 50 nM lapatinib, and found minimal correlation between G_1 and S-G_2 durations (**Fig. 3I**). These experimental observations confirm the implicit assumption of the model that G_1 and S-G_2 durations are uncorrelated.

Lastly, we evaluated model inferences for paclitaxel treatment. Consistent with our experimental observations, the model inferred minimal changes to G_1 and S-G_2 durations (**Fig. 3A**,**J**,**K**). At 2 nM paclitaxel, the model inferred 0.56 cell deaths relative to the starting cell numbers and at 3 nM inferred 0.90 relative cell deaths (**Fig. 3A**, Methods). Experimentally, our observations were consistent with the values inferred by the model: we observed 0.54 and 1.00 relative cell deaths for 2 nM and 3 nM paclitaxel (**Fig. 3L**). To summarize the mechanisms that account for the observed changes in cell numbers due to paclitaxel treatment, we compared the number of cell death events against final cell counts for each of the other drugs. These data show the relative bias of paclitaxel toward inducing cell death, especially at 2 nM, compared to 5 nM gemcitabine and 50 nM lapatinib, which both resulted in similar final cell numbers (**Fig. 3M**). Overall, the LCT model captured key observations about the cell cycle effects of each drug, which were confirmed by new in-depth single cell-tracking of the experimental data.

Responses to drug combinations are dependent on drug specific cell cycle and cell death effects

Durable and effective cancer treatments frequently require administration of multiple drugs, however identification of the principles underlying optimal drug combinations has been challenging[29]. Here, we tested the idea that our LCT model, which incorporates cell cycle effects, can be used to predict the impact of different drug combinations on cell cycle behavior and final cell numbers. We compared two strategies in accounting for drug combination effects. In the first, we combined drug effects on the rates of G_1 and S-G_2 progression using Bliss additivity and assumed the rates of cell death additively combined. In the second, we assumed an additive combination through use of the drug effects on overall cell numbers. To explore these predictions, we varied the dose of one drug in the two drug combination pair and analyzed responses to drug combinations that targeted either the same cell cycle phase (G_1 and G_1, or S-G_2 and S-G_2) or different cell cycle phases (G_1 and S-G_2).

First, we tested combining the rates for two G_1 targeted drugs, such as lapatinib and palbociclib. The model predicted that effects on cell number would saturate around the initial starting cell number, indicating cytostatic effects of this drug combination (**Fig. 4A**). In contrast, drug combination effects based on cell numbers alone predicted a cytotoxic effect at higher drug concentrations, resulting in a reduction in cell numbers relative to the starting cell numbers. We tested these drug combinations experimentally and found a cytostatic effect at higher doses, which matches the model prediction based on combining rates of cell cycle progression (**Fig.4A**).

Next, we analyzed predictions of gemcitabine combined with doxorubicin, which both extend S-G_2 durations and induce cell death (see **Fig. 3A**). We found that combination predictions based on rates and cell counts both predicted a reduction in cell numbers relative to each drug on its own, which we also observed experimentally (**Fig. 4B**).

Lastly, we used the LCT model to examine the impact of combining two drugs that target different cell cycle phases, which mimics lapatinib (G_1 effect) combined with gemcitabine (S phase effect). The cell cycle model predicted an antagonistic effect at higher doses, such that 30 nM gemcitabine combined with 100 nM lapatinib is expected to yield a similar final cell number as 30 nM gemcitabine on its own (**Fig. 4C**). Experimentally, we observed that three of the four lapatinib and gemcitabine combination doses showed an antagonistic impact on cell number when compared against gemcitabine doses on its own. These antagonistic effects of the combination held when lapatinib was replaced by palbociclib, which also impacted G_1 durations (**Fig. 4D**).

We examined the model predictions in more detail to gain insights into the underlying biological mechanisms driving drug combination responses. The LCT model predicted that the G_1 effect of lapatinib would initially dominate over the S-phase effects of gemcitabine, leading to an increased G_1 proportion for the population, in contrast to the balanced G_1 and S phase effects observed in the control condition, which were confirmed experimentally (**Fig. 4E**). In summary, these data indicate that the cell cycle phase and cell death impacts of each drug in a pair are critical for determining the outcome of different drug combination strategies.

DISCUSSION

In this report we link cell cycle regulatory mechanisms with drug specific cell cycle effects to understand how cancer cells respond to individual drugs and drug combinations. To meld these ideas, we developed a combined experimental and modeling approach to measure cell dynamics and infer cell behavior. These approaches revealed that assessment of temporal dynamics and cell behavior are critical to interpret and model drug-induced effects.

Recently, an in-depth analysis revealed that cell cycle phases in individual cells are not correlated, which indicates that the cell cycle should be viewed as a series of uncoupled, memoryless phases rather than as a single process[5,30]. In this work, we found similar uncorrelated patterns in cell cycle phase responses after treatment with different anti-cancer drugs. This revealed multiple implications for assessing and modeling drug responses. First, with a single cell cycle process, cell behavior is assumed to be immediately impacted upon drug treatment; however, we and others have reported that drug effects are often not observed until individual cells enter or approach a drug specific phase or checkpoint[31,32]. For instance, here we found that cells were initially distributed across all phases of the cell cycle, and that addition of lapatinib, a G_1-targeting drug, did not initially affect cells in S-G_2 phase. This led to a partial cell cycle synchronization across the population and required incorporation of a linear chain trick into our model to account for this dwell time. Additionally, the immediate behavioral effect was an important consideration for gemcitabine with lapatinib co-treatment. If both drugs had immediate effects on cell behavior, then we would expect that the G_1 and S-G_2 effects of each drug would counteract each other and lead to a constant ratio of cells in G_1 phase. Instead, both experimentally and through model predictions, we found an initial G_1 enrichment. This likely induced a secondary effect by reducing the relative time that each cell spent in S-phase, which further modulated gemcitabine sensitivity. This finding could explain the antagonistic effects on cell numbers that we and others have observed when combining gemcitabine with lapatinib or palbociclib[33,34]. We speculate that a synergistic effect on cell numbers could also arise by combining two drugs that target S-G_2 phases, where each drug acts to extend the relative duration that each other is effective.

A second implication from having multiple independently regulated processes relates to the concept of effect equivalence in drug combinations. This concept that two drugs with independent targets can be used to identify drug synergy or drug antagonism has predominantly focused on the cell number effect of each drug[8,10–12]. Our current work suggests that equivalence in effect may be better applied to rates of cell cycle phase progression and cell death. In our work we found that lapatinib and palbociclib primarily impacted G_1 phase with limited effects on cell death. In contrast, doxorubicin and gemcitabine extended S-G_2 durations and induced cell death. These cell cycle and cell death effects were critical for drug combinations as we found that the two cytostatic drugs, lapatinib and palbociclib, were additive up to doses that reached the maximum cytostatic effect, and that further dose increases had only minor effects on cell numbers. In contrast, combining the two cytotoxic drugs led to increasingly cytotoxic responses across the full dose range. These results suggest that considering the cell cycle and cell death impacts of each drug is necessary to make predictions about the effects of their combination[35,36].

Drug response measurements evaluated in the context of a computational model can reveal useful information about the nature of drug response and resistance. For instance, a model for the proliferation dynamics of cancer cells can separate the contribution of dividing, non-dividing, and dying cells[20], revealing that the rates of cell death and entry into quiescence change with drug treatment. Previous computational models of cell cycle behavior have explored various ways in which cell cycle behavior impacts drug response but have struggled to use these

models in analysis of drug response. Others have appreciated that drugs do not affect the cell cycle uniformly and have therefore proposed partitioning the cell cycle into multiple independent steps[5], including models in which the cell cycle has several independent, exponentially distributed partitions but which did not capture cell death effects[30]. Modeling cell lifetimes as being hypo-exponentially distributed has helped explain the distribution of cell lifetimes within a population but without connection to known cell cycle stages[37]. In this report, we demonstrate that partitioning known cell cycle phases to account for their dwell-time effects, and including known drug effects like cell death, results in a modeling strategy that can faithfully capture experimentally observed anti-cancer drug effects.

While our model could explain many of the key observations in our experimental data, extensions of the model could could improve its generalizability and robustness. We partitioned the cell cycle into two observed phases, G_1 and S-G_2, which were further subdivided to explain the dwell-time behavior of each phase. With improved reporter strategies[38], we may be able to further subdivide these phases into constituent parts, which could help to localize the effect of a drug to a more specific portion of one cell cycle phase. While the subdivisions within each cell cycle phase are phenomenological, it is tempting to imagine they represent mechanistic steps within each phase. Identifying how effects connect to actual biological events in the cell cycle would help identify opportunities for drug combinations. A practical challenge when using the model for drug combinations has been normalization between experiments. While cell number measurements are routinely normalized by dividing by a control, experiment-to-experiment variation in inferred rates requires additional consideration. A wider panel of experiments, across multiple cell lines, may help to tease apart variation associated with drugs, cell lines, or experiments. A final potential extension is considering the existence of phenotypically diverse subpopulations[39]. At the cost of additional complexity, one could employ several instances of the current model with transition probabilities between these states when the cells divide to simulate a heterogeneous population of cells.

Summary

We observed that five commonly used cancer drugs each modulated cell numbers through distinct routes and with different temporal dynamics. By revealing how these drugs uniquely impacted cell fate, our model and analyses have implications for how different cancer drugs can be combined to maximize therapeutic impact. For example, by suggesting particular drug combinations that modulate cell cycle effects in orthogonal ways, or by suggesting drug schedules that take advantage of the shift in cell cycle state of the overall population. In summary, these studies provide a map for understanding how cancer cells respond to treatment and how drugs may be combined and timed for maximal effect.

ACKNOWLEDGEMENTS

These studies were supported by NIH research grants U54-CA209988, U54-HG008100, U01-CA215709, Prospect Creek Foundation, Jayne Koskinas Ted Giovanis Foundation for Health and Policy, and Breast Cancer Research Foundation.

METHODS

Creation of Stable Cell Lines

AU565 cells (ATCC CRL 2351), were grown in DMEM supplemented with 10% FBS. The coding fragment for clover-HDHB was cloned in frame into a transposase expression plasmid modified to also express a nuclear localized mCherry[40]. The stable cell line was created as previously described[41] and selected for 7 days with 0.75 µg/ml puromycin. Cells were validated by STR profiling as being AU565 cells and tested negative for mycoplasma.

Drug Dose Response Protocol

AU565 cells were plated at a density of 25,000 cells per well into 24-well Falcon plates (Corning #353047). 24H after plating the media was exchanged with Fluorobrite media supplemented with 10% FBS, glutamine, and penicillin-streptomycin. Cells were then treated with dose-escalation: Lapatinib (Selleckchem #S1028), gemcitabine (#S1149), paclitaxel (#S1150), doxorubicin (#S1208), and palbociclib (#S1116). After drug addition, the plates were imaged every 30 minutes for 96H using phase, GFP, and RFP imaging channels with the IncuCyte S3. For single drug treatments only, at 48H the media was replaced, and fresh media and drug were added. Four equally spaced image locations per well and three biological replicates were collected.

Automated Analyses

Phase, GFP, and RFP images were overlaid and collated into single files using FIJI[42], then segmented into three classes (nuclei, background, debris) using a trained classifier in Ilastik[43]. The Ilastik segmented images and IncuCyte GFP images were used to count nuclei and determine cell cycle phase with Cell Profiler[44].

Manual Analyses

To manually track cells, GFP image sequences were registered using the FIJI plug-in 'StackReg'. Individual cells present in the first image and their progeny were followed to identify the time of G_1 transition, apoptosis, and cell division using the plug-in mTrackJ[45]. We excluded cells that were binucleated, had abnormally large nuclei, or were near the image border where complete lineages could not be tracked. The G_1 transition was defined as the last frame before the nuclear intensity of the cell cycle reporter was below the level of the cytoplasm.

Data Pre-processing

The data included the percentage of cells in G_1 phase, and the total number of cells normalized to the cell numbers at the initial time point. We assumed 1 starting cell at t = 0H while calculating the number of cells in G_1 and S-G_2 phase over time. Savitzky-Golay filter was used to smoothen the data. The three replicates of each experiment were averaged, and the average was used for the purpose of fitting.

Core Model

To identify the dynamics of the AU565 cancer cell population in response to compounds, we built a system of ordinary differential equations (ODEs) with two states: G_1, and S-G_2. Cells transition from G_1 to S-G_2 phase, and then vice versa when doubling. Cell death can occur in either phase with phase-specific death rates. S and G_2 phases are combined as our reporter cannot distinguish them. From single-cell tracking, we identified that G_1 and S-G_2 phase time-intervals are Erlang-distributed. Based on this observation, we employed the linear chain trick (LCT)[46] to capture these waiting time distributions. We broke down each phase into a series of sequential sub-phases and derived the system of mean-field ordinary differentials. Each sub-phase is represented as a single state variable within the differential equation system. The total number of cells in each phase is

the sum of the cell numbers in each sub-phase. Furthermore, to account for the non-uniform effect of the drugs over each cell cycle phase, we divided G_1 and S-G_2 into 4 and 4 parts, respectively, such that the effect of a drug can be distinguishable at the beginning, middle, or the end of the phases.

The mean-field system of ODEs is:

$$\frac{d\,G_{11,1}}{dt} = +2\beta_4 G_{24,5} - (\alpha_1 + \gamma_{1,1})G_{11,1}$$
$$\frac{d\,G_{1k,1}}{dt} = +\alpha_{k-1} G_{1k-1,2} - (\alpha_k + \gamma_{1,k})G_{1k,1}$$
$$\frac{d\,G_{1k,2}}{dt} = +\alpha_k G_{1k,1} - (\alpha_k + \gamma_{1,k})G_{1k,2} \qquad 1 \le k \le 4$$

$$\frac{d\,G_{21,1}}{dt} = +\alpha_4 G_{14,2} - (\beta_1 + \gamma_{2,1})G_{21,1}$$
$$\frac{d\,G_{2i,j}}{dt} = +\beta_i G_{2i,j-1} - (\beta_i + \gamma_{2,i})G_{2i,j} \qquad 2 \le j \le 5\,, 1 \le i \le 4$$

The parameters of the model include progression rates through G_1 phase, α, and S-G_2 phase, β, and death rates in each of the G_1 phase, γ_1, and S-G_2 phase, γ_2. Cells at the end of the S-G_2 phase divide and give birth to two cells at G_1 phase. Since each phase is divided into 4 parts, each part in G_1 will contain 2 sub-phases, and each part in S-G_2 will contain 5 sub-phases.

The model was implemented in Julia v1.5.3. The differential equations were solved by the matrix exponential. As the data was measured with equal spacing, we pre-calculated the transition matrix between timesteps.

Dose Response Relationship

We assumed that the progression and death rates in G_1 and S-G_2 that form the quantified drug effects on the population follow a Hill function:

$$Hill\,(C) = E_{min} + \frac{E_{max} - E_{min}}{(1 + \frac{EC50}{C})^k}$$

where the EC_{50} indicates the half-maximal drug effect concentration, E_{min} the value of the rate parameter in the absence of drug, E_{max} the rate parameter at infinite concentration, and k the steepness of the dose-response curve. Given these parameters and the drug concentration (C) we then calculated the specific rate parameters for that treatment.

Exponential Model

To show the benefit of our LCT model, we used a commonly used exponential model to fit to the G_1 and S-G_2 cell numbers and showed the exponential model cannot capture the dynamics of the data. The parameters the same as the mean-field model.

$$\frac{d\,G_1}{dt} = +2\beta G_2 - (\alpha + \gamma_1)G_1$$
$$\frac{d\,G_2}{dt} = +\alpha G_1 - (\beta + \gamma_1)G_2$$

Model Fitting

To simplify the model, we enforced that some parameters are shared across different concentrations of a drug. The shared parameters include the EC_{50} and steepness of the curve. These parameters are drug-specific, but not concentration-specific. Additionally, the number of G_1 and S-G_2 subphases, and the parameters in the absence of drug were shared across all drugs and concentrations. The sum of squared error was used as the cost function value and was calculated between the cell numbers predicted by the model and the average cell numbers of three replicates, over all time points, concentrations, and drugs tested. This cost function was then minimized using the default adaptive differential evolution optimizer from the BlackBoxOptim.jl Julia package, version 0.5.0.

To characterize the identifiability of our fit parameters we conducted a local sensitivity analysis. To do so, we calculated the cost function while varying each parameter from 0.1 to 10 times the optimal value, holding all the other parameters at their optimum (results not shown).

Calculating relative number of cell deaths and average phase durations

We evaluated the number of dead cells at 96H relative to the starting cell number at 0H. This formed the observed relative cell death numbers reported in Figure 3A. To calculate the corresponding cell death values inferred from the model, we calculated the predicted number of cells at each phase part (G_{11}, G_{12}, G_{13}, G_{14}, G_{21}, G_{22}, G_{23}, G_{24}) separately, and multiplied them by their phase part's cell death rate at all time points. The sum of cell numbers died in each phase part gives us the total cell death at each time point, $n(t)$. Integrating over 96H results in total cell death numbers N. Since the initial cell number is 1, this value refers to the relative predicted cell death number reported in Figure 3A.

$$n(t) = \sum_{i=1}^{2}\sum_{j=1}^{4} G_{ij}(t) \times \gamma_{ij}$$

$$N = \sum_{t=0}^{T} n(t)$$

The average phase durations ($\overline{G_1}$,$\overline{S-G_2}$) from the model were calculated using the progression rates. The progression rates are in the unit of the number of subphases over time. The G_1 phase has 8 subphases which is divided into 4 parts that results in 2 phases per part. S-G_2 phase has 20 subphases divided into 4 parts that results in 5 subphases in each part. Each phase part has a unique parameter for cell death and phase progression rate. The average phase duration will be given by the following expressions.

$$\overline{G_1} = \sum_{j=1}^{4} \frac{2}{\alpha_{1j}}$$

$$\overline{S-G_2} = \sum_{j=1}^{4} \frac{5}{\beta_{2j}}$$

Predicting Drug Combinations

Bliss independence was used to calculate the predicted effect of drug combinations. Assuming $E_a$and E_b to be the saturable, quantified effects of drugs a and b, the expected combined effect would be:

$$E_{ab} = E_a + E_b - E_a.E_b \qquad (*)$$

For death effects, we added the effects of individual drugs to find the death effect of drug combination:

$$D_{ab} = D_a + D_b \qquad (**)$$

The Bliss relationship requires that data first be scaled to be between 0 and 1, and then scaled back after the interaction calculation:

$$\hat{X} = \frac{(X_{control} - X)}{X_{control}}$$

This measure is usually used as a baseline to decide whether the combination of two drugs is synergistic or antagonistic. Here we used Bliss in two ways; (1) on the progression rate parameters to simulate the model predictions of drug combinations, and (2) on cell numbers to serve as a baseline of traditional way of calculating drug combination. In the first case, we use Bliss additivity on the cell cycle progression rates (*) to find the set of progression parameters representing the combined drug and assume that the death effects are only additive because the cell death process is not saturable (**). The combination parameters for all the eight concentrations for all pairs of drugs were calculated and then converted back to their original units. Next, we simulated the cell numbers using these parameters. In the baseline case, we used the cell numbers in control condition to normalize the cell number measurements and then converted the cell numbers back to their original scale. This was used as a benchmark reference.

Data Availability

Data was deposited to the Image Data Resource (https://idr.openmicroscopy.org) under accession number idr0119. All other data and analyses used in this study are available from the corresponding author upon reasonable request.

Code Availability

The code and analysis can be found at https://github.com/meyer-lab/DrugResponseModel.jl.

FIGURE LEGENDS

Figure 1. Population responses to drugs vary with dose, time, and cell cycle. A. Schematic of reporter with a bidirectional promoter driving expression of human DNA Helicase B (HDHB) fused to the green fluorescent protein clover, and a second transcript coding for NLS-RFP-NLS, a ribosome skipping domain (T2A), and a puromycin resistance protein. **B.** Quantification of nuclear intensity of the cell cycle reporter in a cell and its progeny across time. The time of G_1/S transition and cell division are demarcated with black and red circles respectively. **C.** Schematic of the five drugs tested and the cell cycle phase they target. **D.** Average growth curves of AU565 cells tracked every 30 min for 96hr across an 8-point dose response for lapatinib, gemcitabine, paclitaxel, palbociclib, and doxorubicin. The null dose is colored red. Line traces show the average from three independent experiments. The black triangle indicates the addition of fresh drug and media. **E.** Percentage of cells in S-G_2 phase of the cell cycle across doses. 50 nM Lapatinib and 3 nM paclitaxel are colored blue. **F.** GFP images at 39.5H for 250 nM lapatinib, 30 nM gemcitabine, 3 nM paclitaxel, 250 nM palbociclib, 20 nM doxorubicin.

Figure 2. A dynamical model of the cell cycle captures the dynamics of drug response. A. Diagram of the phase transitions in a cell cycle. α_1, α_2, α_3 , and α_4 are the progression rates

through G_1 phase, β_1, β_2, β_3, and β_4 are the progression rates through the 4 parts of S-G_2. Similarly, γ_{11}, γ_{12}, γ_{13}, and γ_{14} are the death rates through the G_1 phase parts, and γ_{21}, γ_{22}, γ_{23}, and γ_{24} are death rates through S-G_2 phase parts. **B.** The sum of squared errors for the fits of each of five drugs over all concentrations with and without the LCT modification. **C-D.** G_1 and S-G_2 cell numbers overtime, respectively, for the control and lapatinib treatment at 5 concentrations (solid lines), overlayed with the average of three experimental replicates (dashed lines). **E-F.** The average phase durations in G_1 and S-G_2 phases for all five drug treatments. The arrow shows the shift from the control condition to the drug effect at the half maximum concentration (E_{EC50}). **G-H.** G_1 and S-G_2 cell numbers of gemcitabine treatment over time. **I-J.** The overall probability of cell death in G_1 and S-G_2 phase, respectively, for all five drug treatments. The arrow shows the shift from the control condition to the drug effect at the half maximum concentration (E_{EC50}) for G_1 and S-G_2 phases. **K-L.** The predicted accumulated dead cells over time for lapatinib and gemcitabine treated cells, respectively, for control condition and 5 other concentrations. The relative cell numbers at the predicted EC_{50} at T=96H are lapatinib=0.97, doxorubicin=1.62, gemcitabine=1.69, paclitaxel=1.53, Palbociclib=2.19.

Figure 3. Analysis of single cell responses confirms model inferences and reveals drug-specific cell cycle phase effects. A. Quantification of cell cycle parameters as inferred by the model and observed experimentally ($G_1$and S-G_2 durations and cell death). **B.** Distributions of G_1 durations for cells that underwent one division in response to 0, 25, and 50 nM lapatinib. **C.** Distributions of S-G_2 durations. **D.** Accumulated cell death across time. **E.** Time to first division for cells in the CTRL condition (red line) compared to 50 nM lapatinib (gray line). **F-H.** G_1 and S-G_2 distributions, and cell death accumulation in response to gemcitabine. **I.** G_1 and S-G_2 durations for the first complete cell cycle for all cells tracked in the control condition, in response to 100 nM lapatinib, and 10 nM gemcitabine. **J-L.** G_1 and S-G_2 distributions, and cell death accumulation in response to paclitaxel. **M.** Observed cell counts against cell deaths per drug.

Figure 4. Responses to drug combinations are dependent on drug specific effects on the cell cycle and cell death. A-D. Comparison between model predictions for single drug responses, or from drug combinations of Bliss additivity using cell numbers or model rates. **A.** Single drug responses for increasing doses of palbociclib and in combination with 100 nM lapatinib. **B-D.** Single drug responses for increasing doses of gemcitabine and in combination with 20 nM doxorubin, 100 nM lapatinib, 50 nM palbociclib. **E.** Model predictions for the percentage of cells in G_1 phase for the control condition, 100 nM lapatinib, 17 nM gemcitabine, or the combination of lapatinib and gemcitabine. **E-H.** Comparison between the actual experiments for the single drug responses and the drug combinations as described in panels A-D. Error bars show the standard error of the mean for three biological replicates.

Figure S1. An exponential cell cycle model without incorporating delay times fails to capture the dynamics of drug response. A. The transition diagram for a simple dynamical model with 2 phases (G_1 and S-G_2) and without the LCT. α and β, are the transition rates from G_1 to S-G_2 and vice versa, γ_1 and γ_2 are the death rates in G_1 and S-G_2, respectively. **(B-E).** Exponential cell cycle model simulations of G_1 and S-G_2 cell numbers over time for control and 5 concentrations of lapatinib **(B-C)** and gemcitabine **(D-E)** (solid lines), respectively, overlayed with the average of three experimental replicates (dashed lines).

Figure S2. A dynamical model of the cell cycle captures the dynamics of drug response. A-F. G_1 and S-G_2 cell numbers overtime, respectively, for the control and treatment at 5 concentrations (solid lines) for doxorubicin (**A-B**) paclitaxel (**C-D**), and palbociclib (**E-F**) overlayed with the average of three corresponding experimental replicates (dashed lines). (**G-L**) The average phase durations in G_1 and S-G_2 phases for all five drug treatments. The arrow

shows the shift from the control condition to the drug effect at the half maximum concentration (E_{EC50}).

Figure S3. Analysis of single cell tracking data reveals drug-specific cell cycle phase effects. A. Lineage trees of 25 lineages across 96H for various drug treatments. Tracks are colored coded based on cell cycle phase: gray indicates G_1 and red indicates S-G_2 phase. Track splitting indicates mitosis, and track ending prior to 96H corresponds to apoptosis. **B.** Quantification of cell outcomes (division, apoptosis, still present at end of experiment) for cells from the first and second generations treated with lapatinib, gemcitabine, or paclitaxel. **C.** Gamma distribution of G_1 and S-G_2 phase durations for cells in control condition with sample size of 520 and 514 for G_1 and S-G_2 phases, respectively.

REFERENCES

1. Sancar, A., Lindsey-Boltz, L. A., Ünsal-Kaçmaz, K. & Linn, S. Molecular mechanisms of mammalian DNA repair and the DNA damage checkpoints. *Annual Review of Biochemistry* (2004) doi:10.1146/annurev.biochem.73.011303.073723.
2. Hartwell, L. H. & Weinert, T. A. Checkpoints: Controls that ensure the order of cell cycle events. *Science (80-.).* (1989) doi:10.1126/science.2683079.
3. Barnum, K. J. & O'Connell, M. J. Cell cycle regulation by checkpoints. *Methods in Molecular Biology* (2014) doi:10.1007/978-1-4939-888-2_2.
4. P, L.-G., FG, W. & SS, T. The spindle assembly checkpoint. *Curr. Biol.* **22**, (2012).
5. HX, C. *et al.* Evidence that the human cell cycle is a series of uncoupled, memoryless phases. *Mol. Syst. Biol.* **15**, (2019).
6. RS, F. *et al.* PD 0332991, a selective cyclin D kinase 4/6 inhibitor, preferentially inhibits proliferation of luminal estrogen receptor-positive human breast cancer cell lines in vitro. *Breast Cancer Res.* **11**, (2009).
7. P, H. & W, P. Fludarabine- and gemcitabine-induced apoptosis: incorporation of analogs into DNA is a critical event. *Cancer Chemother. Pharmacol.* **36**, 181–188 (1995).
8. J, O. *et al.* An Unbiased Oncology Compound Screen to Identify Novel Combination Strategies. *Mol. Cancer Ther.* **15**, 1155–1162 (2016).
9. M, H., M, N., M, C. & PK, S. Growth rate inhibition metrics correct for confounders in measuring sensitivity to cancer drugs. *Nat. Methods* **13**, 521–527 (2016).
10. SL, H. *et al.* The National Cancer Institute ALMANAC: A Comprehensive Screening Resource for the Detection of Anticancer Drug Pairs with Enhanced Therapeutic Activity. *Cancer Res.* **77**, 3564–3576 (2017).
11. MP, M. *et al.* Community assessment to advance computational prediction of cancer drug combinations in a pharmacogenomic screen. *Nat. Commun.* **10**, (2019).
12. CT, M., DJ, W., CF, L. & V, Q. Charting the Fragmented Landscape of Drug Synergy. *Trends Pharmacol. Sci.* **41**, 266–280 (2020).
13. AC, P., C, C. & PK, S. A curative combination cancer therapy achieves high fractional cell killing through low cross-resistance and drug additivity. *Elife* **8**, (2019).
14. A, S., LA, L.-B., K, U.-K. & S, L. Molecular mechanisms of mammalian DNA repair and the DNA damage checkpoints. *Annu. Rev. Biochem.* **73**, 39–85 (2004).
15. Garnett, M. J. *et al.* Systematic identification of genomic markers of drug sensitivity in cancer cells. *Nature* (2012) doi:10.1038/nature11005.
16. Heiser, L. M. *et al.* Subtype and pathway specific responses to anticancer compounds in breast cancer. *Proc. Natl. Acad. Sci. U. S. A.* (2012) doi:10.1073/pnas.1018854108.
17. RH, S. The NCI60 human tumor cell line anticancer drug screen. *Nat. Rev. Cancer* (2006).
18. Hafner, M., Niepel, M., Chung, M. & Sorger, P. K. Growth rate inhibition metrics correct for confounders in measuring sensitivity to cancer drugs. *Nat. Methods* (2016) doi:10.1038/nmeth.3853.
19. LA, H. *et al.* An unbiased metric of antiproliferative drug effect in vitro. *Nat. Methods* **13**, 497–500 (2016).
20. DR, T., SP, G., PL, F. & V, Q. Fractional proliferation: a method to deconvolve cell population dynamics from single-cell data. *Nat. Methods* **9**, 923–928 (2012).
21. SL, S. *et al.* The proliferation-quiescence decision is controlled by a bifurcation in CDK2 activity at mitotic exit. *Cell* **155**, 369 (2013).
22. Wang, T.-H., Wang, H.-S., Soong, Y.-K. & Ph, M. Paclitaxel-Induced Cell Death Where the Cell Cycle and Apoptosis Come Together BACKGROUND. Compelling evidence indicates that paclitaxel kills cancer cells. (2000) doi:10.1002/1097-0142(20000601)88:11.
23. P, H. & W, P. Induction of apoptosis by gemcitabine. *Semin. Oncol.* **22**, 19–25 (1995).

24. Gardner, S. N. A mechanistic, predictive model of dose-response curves for cell cycle phase-specific and -nonspecific drugs. *Cancer Res.* **60**, 1417–1425 (2000).
25. Strogatz, S. H. & Dichter, M. Nonlinear Dynamics and Chaos, 2nd ed. SET with Student Solutions Manual. 932 (2016).
26. Hurtado, P. J. & Richards, C. Building mean field ODE models using the generalized linear chain trick & Markov chain theory. *http://mc.manuscriptcentral.com/tjbd* **15**, S248–S272 (2021).
27. Kwon, Y.-S., Chun, S.-Y., Nam, K.-S. & Kim, S. Lapatinib sensitizes quiescent MDA-MB-231 breast cancer cells to doxorubicin by inhibiting the expression of multidrug resistance-associated protein-1. *Oncol. Rep.* **34**, 884–890 (2015).
28. M, S. & M, S. Palbociclib-The First of a New Class of Cell Cycle Inhibitors. *Recent Results Cancer Res.* **211**, 153–175 (2018).
29. KT, F. *et al.* Combined BRAF and MEK inhibition in melanoma with BRAF V600 mutations. *N. Engl. J. Med.* **367**, 1694–1703 (2012).
30. Vittadello, S. T., McCue, S. W., Gunasingh, G., Haass, N. K. & Simpson, M. J. Mathematical models incorporating a multi-stage cell cycle replicate normally-hidden inherent synchronization in cell proliferation. *J. R. Soc. Interface* **16**, (2019).
31. T, R. *et al.* Cell-Cycle Position of Single MYC-Driven Cancer Cells Dictates Their Susceptibility to a Chemotherapeutic Drug. *Cell Syst.* **5**, 237-250.e8 (2017).
32. HX, C. *et al.* Orchestration of DNA Damage Checkpoint Dynamics across the Human Cell Cycle. *Cell Syst.* **5**, 445-459.e5 (2017).
33. AK, M. *et al.* CDK4/6 inhibition antagonizes the cytotoxic response to anthracycline therapy. *Cell Cycle* **11**, 2747–2755 (2012).
34. JL, D., AK, M. & ES, K. Modification of the DNA damage response by therapeutic CDK4/6 inhibition. *J. Biol. Chem.* **287**, 29075–29087 (2012).
35. SY, B. *et al.* Measurement and models accounting for cell death capture hidden variation in compound response. *Cell Death Dis.* **11**, (2020).
36. R, R. *et al.* Drug antagonism and single-agent dominance result from differences in death kinetics. *Nat. Chem. Biol.* **16**, 791–800 (2020).
37. Yates, C. A., Ford, M. J. & Mort, R. L. A Multi-stage Representation of Cell Proliferation as a Markov Process. *Bull. Math. Biol. 2017 7912* **79**, 2905–2928 (2017).
38. BT, B. *et al.* Fluorescent indicators for simultaneous reporting of all four cell cycle phases. *Nat. Methods* **13**, 993–996 (2016).
39. Meyer, A. S. & Heiser, L. M. Systems biology approaches to measure and model phenotypic heterogeneity in cancer. *Curr. Opin. Syst. Biol.* **17**, 35–40 (2019).
40. Gross, S. M., Dane, M. A., Bucher, E. & Heiser, L. M. Individual Cells Can Resolve Variations in Stimulus Intensity along the IGF-PI3K-AKT Signaling Axis. *Cell Syst.* (2019) doi:10.1016/j.cels.2019.11.005.
41. SM, G., MA, D., E, B. & LM, H. Individual Cells Can Resolve Variations in Stimulus Intensity along the IGF-PI3K-AKT Signaling Axis. *Cell Syst.* **9**, 580-588.e4 (2019).
42. Schindelin, J. *et al.* Fiji: An open-source platform for biological-image analysis. *Nature Methods* (2012) doi:10.1038/nmeth.2019.
43. Berg, S. *et al.* ilastik: interactive machine learning for (bio)image analysis. *Nat. Methods* (2019) doi:10.1038/s41592-019-0582-9.
44. McQuin, C. *et al.* CellProfiler 3.0: Next-generation image processing for biology. *PLoS Biol.* (2018) doi:10.1371/journal.pbio.2005970.
45. E, M., O, D. & I, S. Methods for cell and particle tracking. *Methods Enzymol.* **504**, 183–200 (2012).
46. Hurtado, P. J. & Kirosingh, A. S. Generalizations of the 'Linear Chain Trick': incorporating more flexible dwell time distributions into mean field ODE models. *J. Math. Biol.* (2019) doi:10.1007/s00285-019-01412-w.

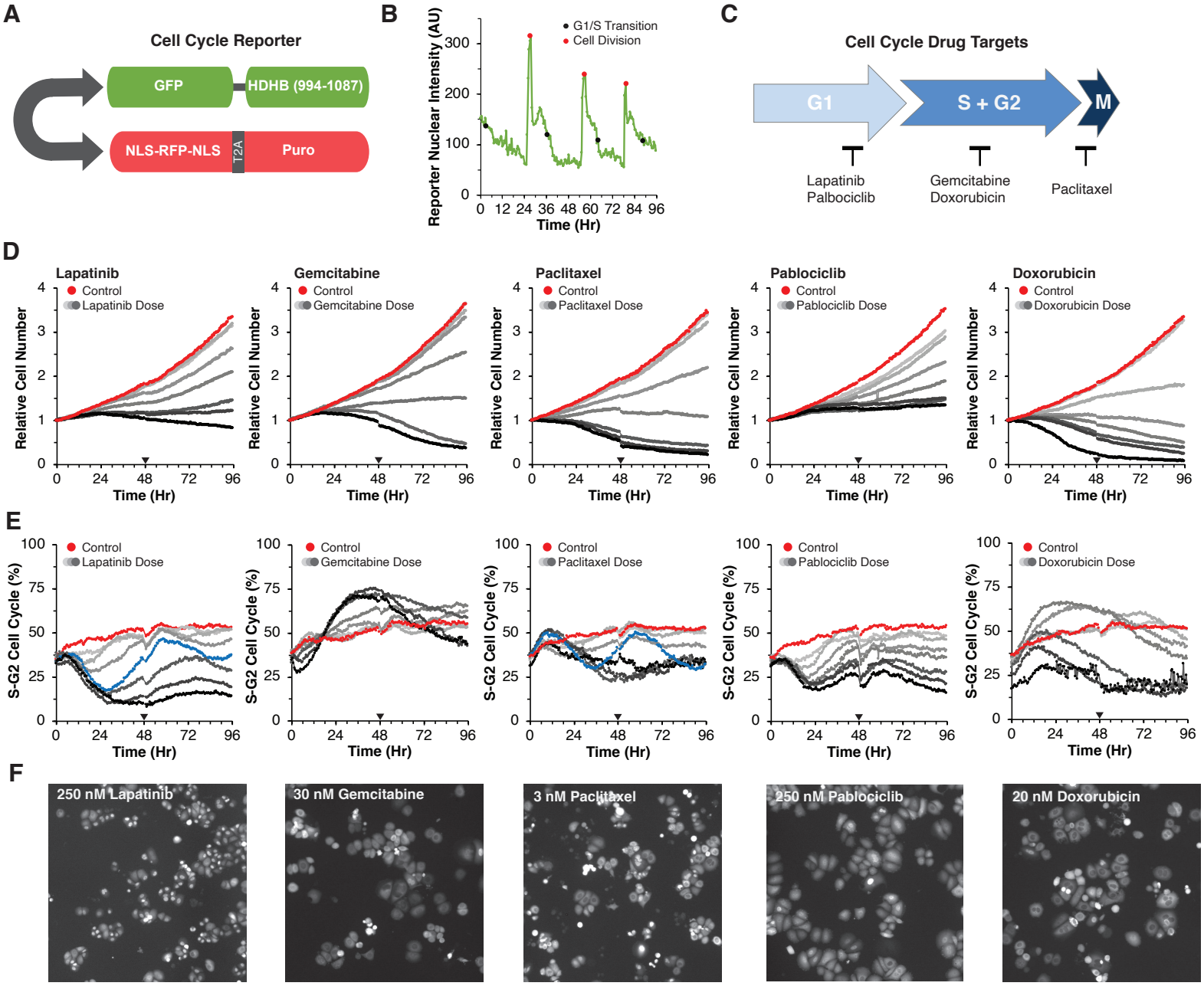
A
Cell Cycle Reporter
GFP
HDHB (994-1087)
NLS-RFP-NLS
T2A
Puro
B
G1/S Transition
Cell Division
Reporter Nuclear Intensity (AU)
Time (Hr)
C
Cell Cycle Drug Targets
G1
S + G2
M
Lapatinib
Palbociclib
Gemcitabine
Doxorubicin
Paclitaxel
D
Lapatinib
Control
Lapatinib Dose
Gemcitabine
Gemcitabine Dose
Paclitaxel
Paclitaxel Dose
Pablociclib
Pablociclib Dose
Doxorubicin
Doxorubicin Dose
Relative Cell Number
Time (Hr)
E
S-G2 Cell Cycle (%)
F
250 nM Lapatinib
30 nM Gemcitabine
3 nM Paclitaxel
250 nM Pablociclib
20 nM Doxorubicin

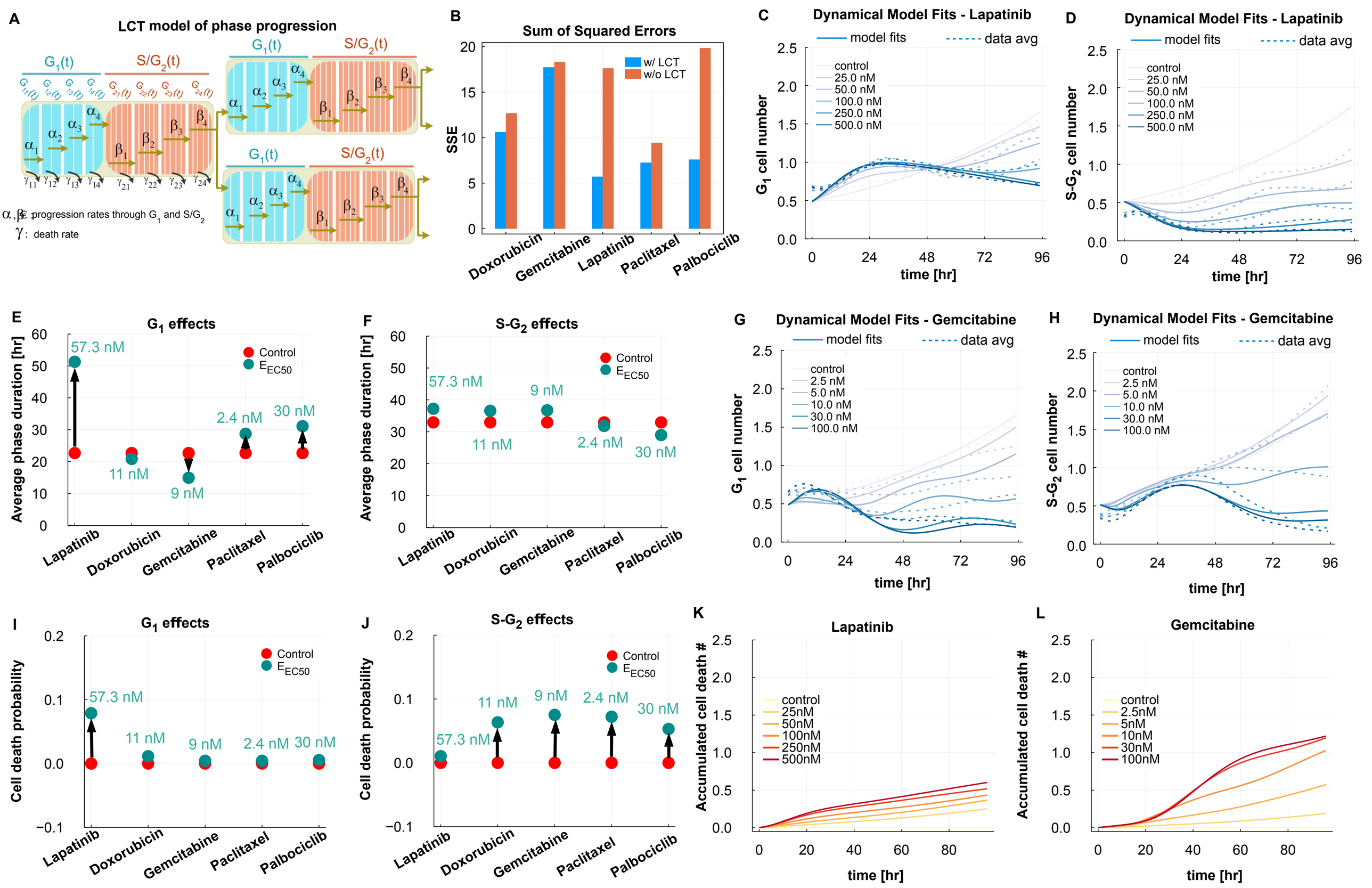
A
LCT model of phase progression
G1(t)
S/G2(t)
α, β: progression rates through G1 and S/G2
γ: death rate
B
Sum of Squared Errors
SSE
w/ LCT
w/o LCT
Doxorubicin
Gemcitabine
Lapatinib
Paclitaxel
Palbociclib
C
Dynamical Model Fits - Lapatinib
model fits
data avg
control
25.0 nM
50.0 nM
100.0 nM
250.0 nM
500.0 nM
G1 cell number
time [hr]
D
Dynamical Model Fits - Lapatinib
S-G2 cell number
E
G1 effects
Average phase duration [hr]
Control
EEC50
57.3 nM
11 nM
9 nM
2.4 nM
30 nM
F
S-G2 effects
G
Dynamical Model Fits - Gemcitabine
control
2.5 nM
5.0 nM
10.0 nM
30.0 nM
100.0 nM
H
Dynamical Model Fits - Gemcitabine
I
G1 effects
Cell death probability
J
S-G2 effects
K
Lapatinib
Accumulated cell death #
control
25nM
50nM
100nM
250nM
500nM
L
Gemcitabine
control
2.5nM
5nM
10nM
30nM
100nM

A

Treatment	G1 Duration Predicted (Hr)	G1 Duration Observed (Hr)	S/G2 Duration Predicted (Hr)	S/G2 Duration Observed (Hr)	Cell Death Predicted (Relative Number)	Cell Death Observed (Relative Number)
Control	22.7	19.4	32.9	22.3	0.00	0.14
Lapatinib 25nM	33.6	26.2	33.2	24.0	0.25	0.06
Lapatinib 50nM	47.4	32.5	36.1	25.2	0.37	0.20
Gemcitabine 5 nM	15.1	18.0	33.3	34.5	0.57	0.14
Gemcitabine 10nM	15.1	20.5	37.8	38.0	1.00	0.41
Paclitaxel 2nM	26.7	21.8	31.4	24.6	0.56	0.54
Paclitaxel 3nM	32.0	22.9	33.7	26.9	0.90	1.00

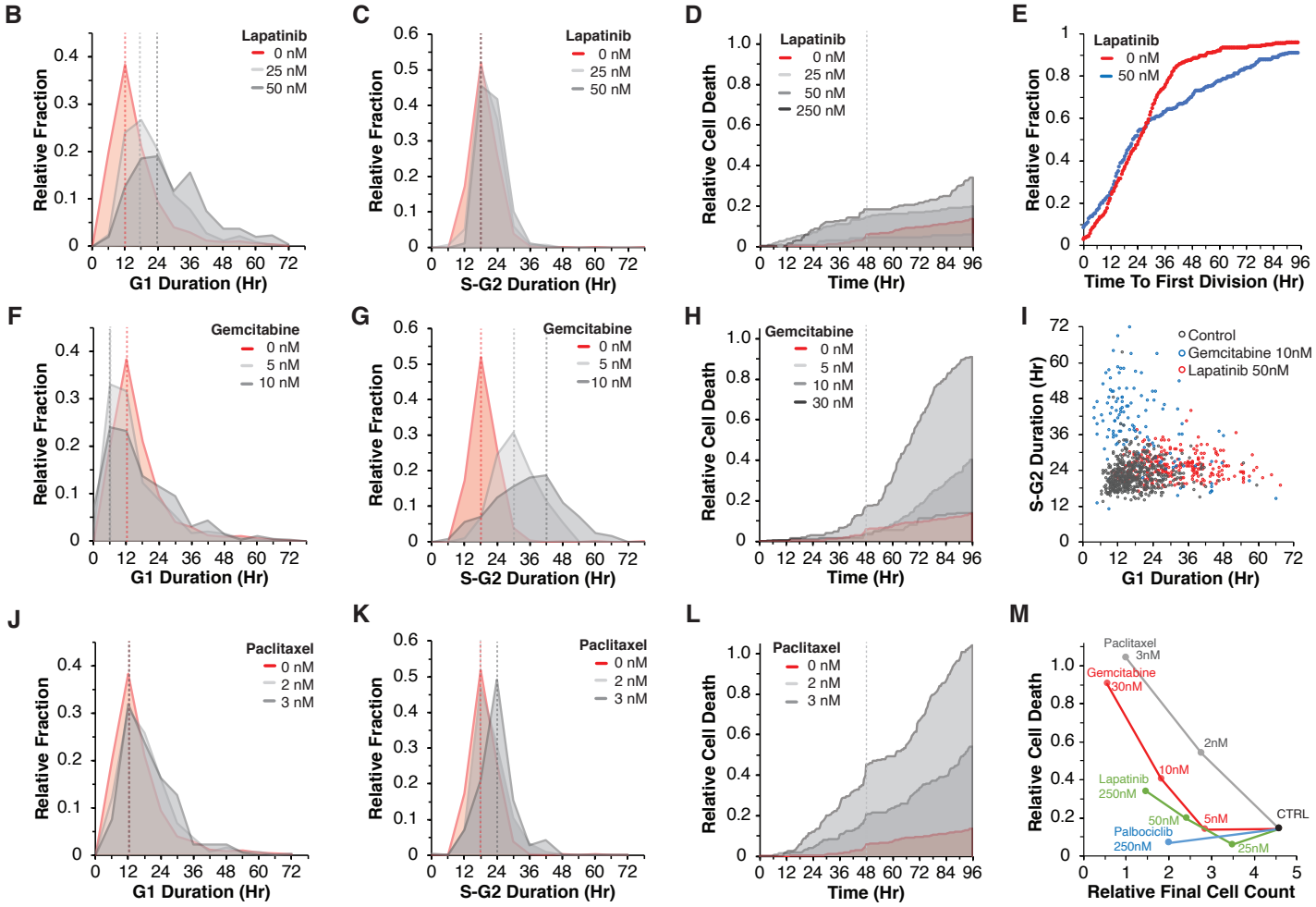

Fig. 4 Drug Combinations

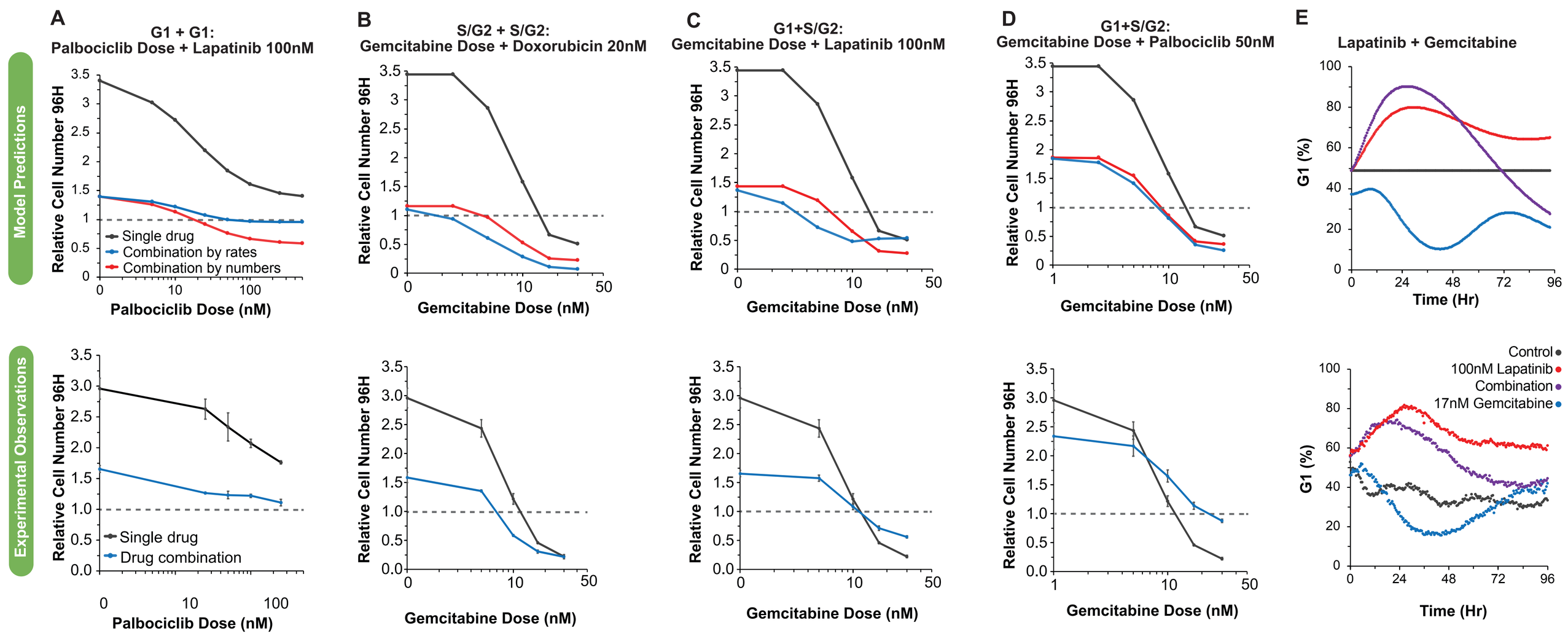

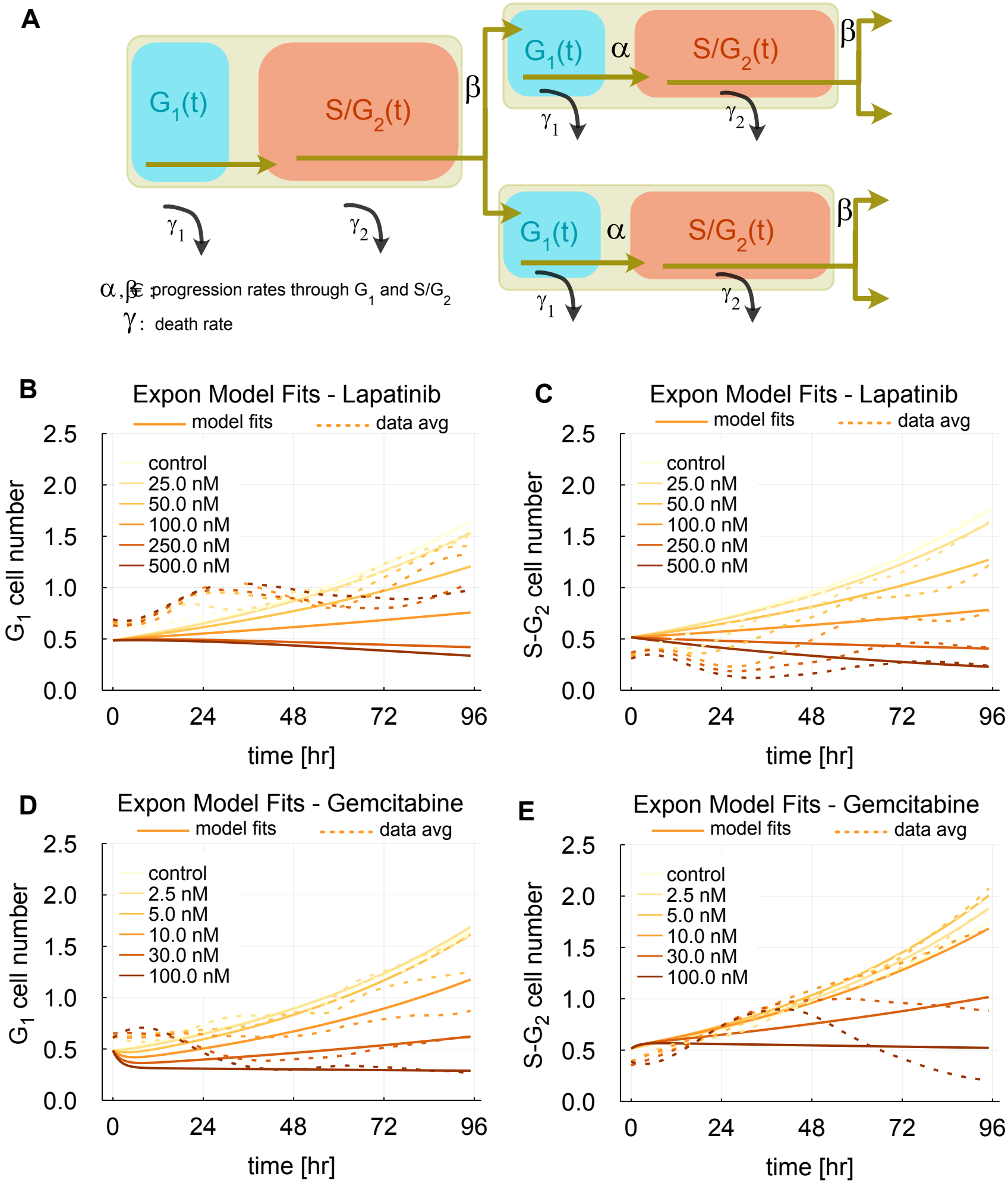
A
G1(t)
S/G2(t)
β
α
γ1
γ2
α, β : progression rates through G1 and S/G2
γ : death rate
B
Expon Model Fits - Lapatinib
model fits
data avg
control
25.0 nM
50.0 nM
100.0 nM
250.0 nM
500.0 nM
G1 cell number
time [hr]
C
Expon Model Fits - Lapatinib
S-G2 cell number
D
Expon Model Fits - Gemcitabine
control
2.5 nM
5.0 nM
10.0 nM
30.0 nM
100.0 nM
E
Expon Model Fits - Gemcitabine

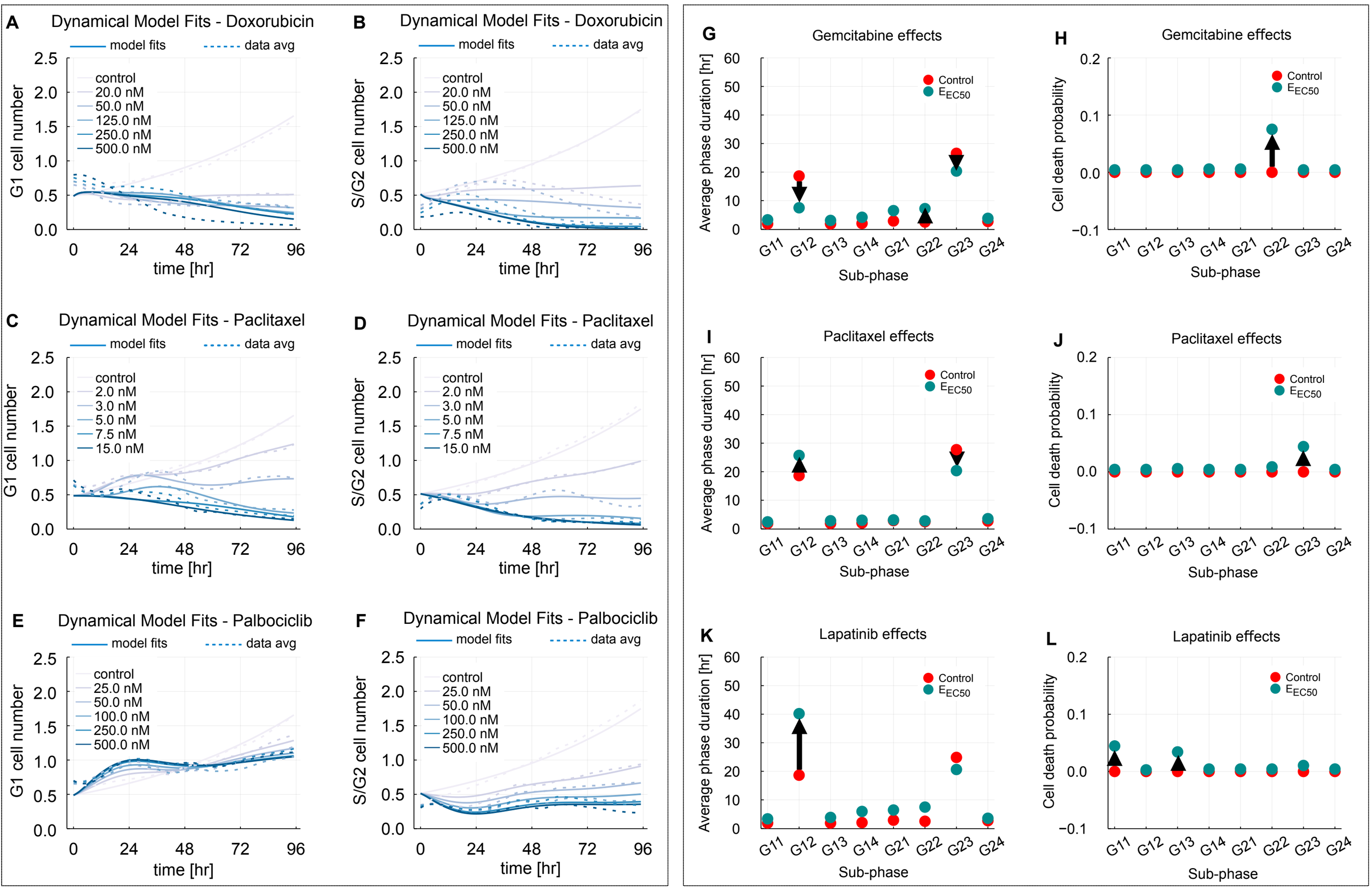
A
Dynamical Model Fits - Doxorubicin
model fits
data avg
control
20.0 nM
50.0 nM
125.0 nM
250.0 nM
500.0 nM
G1 cell number
time [hr]
B
Dynamical Model Fits - Doxorubicin
S/G2 cell number
C
Dynamical Model Fits - Paclitaxel
control
2.0 nM
3.0 nM
5.0 nM
7.5 nM
15.0 nM
D
Dynamical Model Fits - Paclitaxel
E
Dynamical Model Fits - Palbociclib
control
25.0 nM
50.0 nM
100.0 nM
250.0 nM
500.0 nM
F
Dynamical Model Fits - Palbociclib
G
Gemcitabine effects
Average phase duration [hr]
Control
E_{EC50}
Sub-phase
H
Gemcitabine effects
Cell death probability
I
Paclitaxel effects
J
Paclitaxel effects
K
Lapatinib effects
L
Lapatinib effects
G11
G12
G13
G14
G21
G22
G23
G24

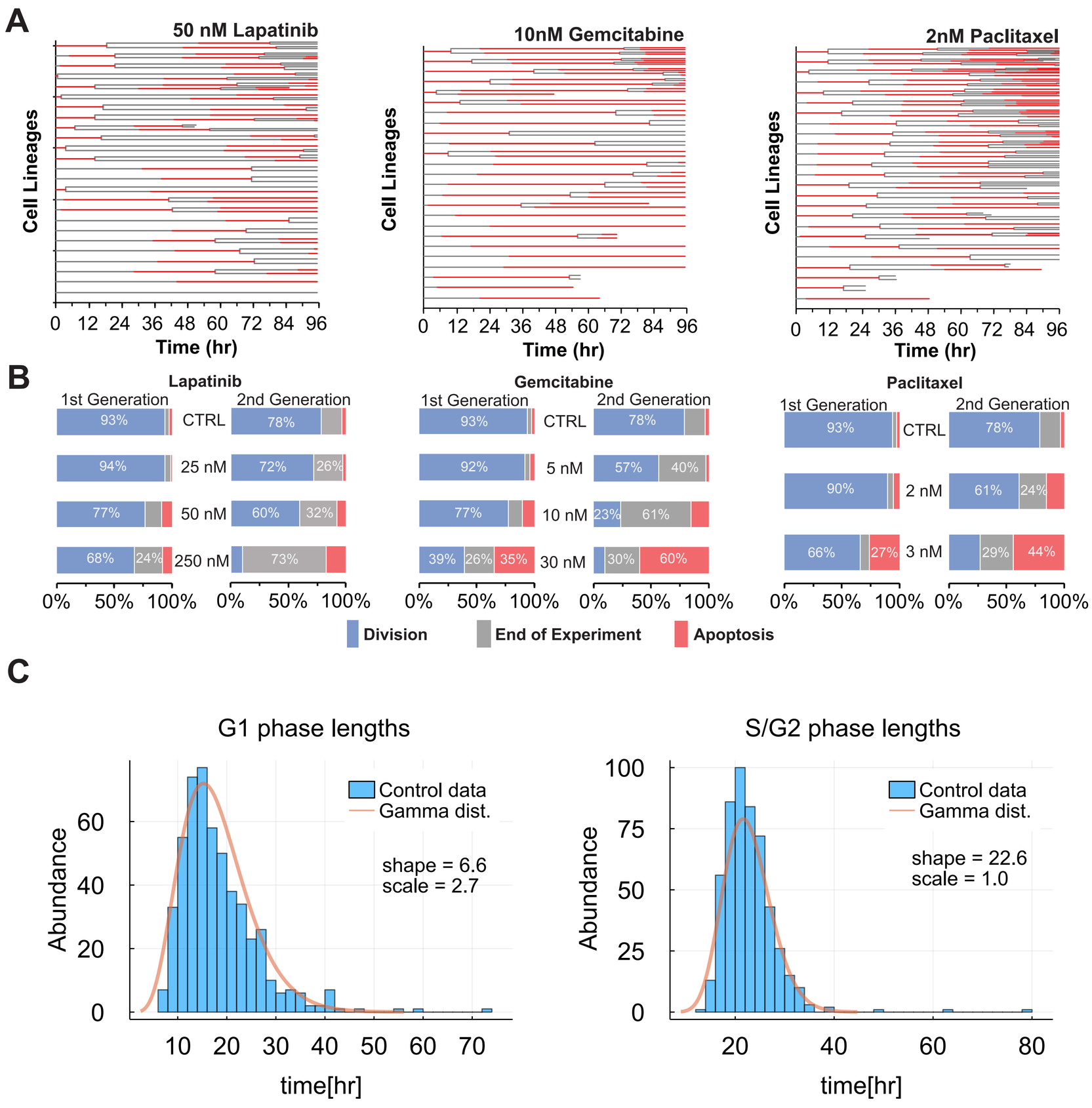
A
50 nM Lapatinib
10nM Gemcitabine
2nM Paclitaxel
Cell Lineages
0 12 24 36 48 60 72 84 96
Time (hr)
B
Lapatinib
Gemcitabine
Paclitaxel
1st Generation
2nd Generation
CTRL
25 nM
50 nM
250 nM
5 nM
10 nM
30 nM
2 nM
3 nM
93%
78%
94%
72%
26%
77%
60%
32%
68%
24%
73%
92%
57%
40%
23%
61%
39%
26%
35%
30%
60%
90%
61%
24%
66%
27%
29%
44%
0% 50% 100%
Division
End of Experiment
Apoptosis
C
G1 phase lengths
S/G2 phase lengths
Control data
Gamma dist.
shape = 6.6
scale = 2.7
shape = 22.6
scale = 1.0
Abundance
time[hr]